Development of Jets rig dedicated for an Active Launch Escape Abort System Wind Tunnel Model

Mihaita Gilbert STOICAN*,[1], Marina ANDREI[1], Tiberiu SALAORU[1], Ionut BUNESCU[1,2], Mihai-Vladut HOTHAZIE[1,2], Mihai Victor PRICOP[1]

*Corresponding author
[1]INCAS – National Institute for Aerospace Research "Elie Carafoli",
B-dul Iuliu Maniu 220, Bucharest 061126, Romania,
stoican.gilbert@incas.ro*, andrei.marina@incas.ro, salaoru.tiberiu@incas.ro,
bunescu.ionut@incas.ro, hothazie.mihai@incas.ro, pricop.victor@incas.ro
[2]Doctoral School of Aerospace Engineering, POLITEHNICA University Bucharest,
Strada Gheorghe Polizu 1, 011061, Bucharest, Romania

DOI: 10.13111/2066-8201.2024.16.2.10

Received: 15 April 2024/ Accepted: 28 May 2024/ Published: June 2024

Abstract: *The development of space launch systems requires rigorous testing and validation of safety mechanisms to ensure the protection of human life and mission-critical assets. One such safety mechanism is the Active Launch Escape/Abort System (ALEAS), designed to swiftly extract crew and spacecraft from a malfunctioning launch vehicle. To evaluate the performance of ALEAS, wind tunnel testing is indispensable. This paper presents the development of a specialized Jets Rig tailored for wind tunnel testing of an ALEAS model. The primary objectives of this research activity include the design, construction, and validation of a Jets Rig that can accurately simulate the propulsion dynamics of an ALEAS system within a wind tunnel environment. The Jets Rig incorporates a special instrumentation and control systems to replicate the complex operational conditions experienced during a launch abort scenario. By achieving this, it enables a comprehensive assessment of ALEAS performance, including thrust duration and plume interaction effects, among others. Key aspects of this study encompass the aerodynamic and structural considerations involved in designing the Jets Rig, the integration of high-fidelity sensors and data acquisition systems, and the development of advanced computational models for predictive analysis. Additionally, the research explores the challenges and solutions associated with the scalability of the Jets Rig to accommodate varying scales of ALEAS models. The findings from this project hold significant implications for advancing the safety and reliability of crewed space missions. A comprehensive understanding of ALEAS performance in a wind tunnel setting allows for the refinement of design parameters, algorithms, and the enhancement of abort system efficiency. Ultimately, the successful development of this dedicated Jets Rig contributes to the broader mission of ensuring the safe exploration of space and the protection of human life in the challenging and dynamic environment of space launch.*

Key Words: *similitude jets, active control jets, CFD, wind tunnel aerodynamics, Active Launch Escape/ Abort System, FEA*

1. INTRODUCTION

The main subject of this paper is the development of a new capability for the trisonic wind tunnel of INCAS which allows for further complex aerodynamic experiments of an active jet

model. The main purpose of this kind of tests is to evaluate the aerodynamic performance of an Active Launch Escape/ Abort System(ALEAS) of a manned space launcher using a sequence of ignition of motors according to the real scenarios of a space mission. These systems are the ultimate safety net for astronauts during the most perilous phase – launch and ascent. Traditional Active Launch Escape system (ALES), like those used on Apollo and Orion, utilize a powerful solid-fueled rocket motor mounted atop the capsule. Alternatively, pusher systems, exemplified by Crew Dragon's Super-Draco engines integrated at the base, offer a sleeker profile but may have limitations on abort scenarios during very low altitude launches. Escape motor thrust profiles are designed to overcome the launch vehicle's acceleration and propel the capsule to a safe distance, ensuring astronaut survival during a catastrophic failure. The Active Launch Abort System (ALAS) needs to be able to initiate an abort throughout the critical ascent phase, encompassing liftoff, transonic acceleration, and reaching a safe altitude and dynamic pressure window. This necessitates robust abort initiation criteria and redundant flight control systems to ensure crew escape from a potential disaster. Multiple sensors and independent abort paths are a cornerstone of these systems. This redundancy maximizes the chances of crew survival in case of primary system failure. Fault tolerance and fail-operational design principles are paramount for these life-critical systems.

The ALEAS consists of an ogive-conical fairing surrounding the Crew Module (CM), an abort motor dedicated for different altitude of abort scenario (LM and HM) to provide the main propulsive force to accelerate the vehicle, a jettison motor (JM) to separate the LAS from the CM once the vehicle is clear of the launch vehicle, and an Low/High Altitude Control Motors (LACM/HACM) which provide the steering torques for the Launch Abort Vehicle (LAV).

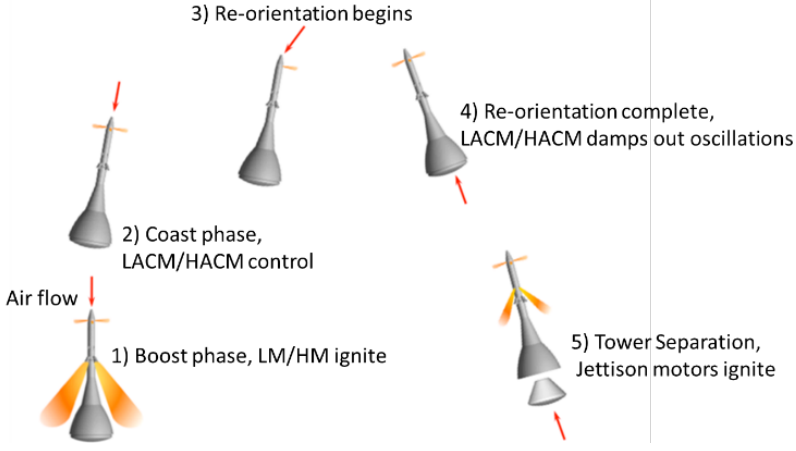

Figure 1. Typical abort sequence [1]

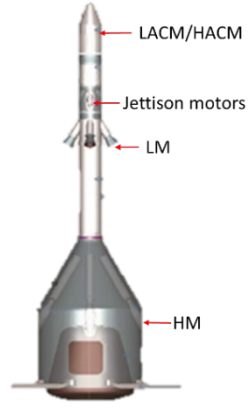

Figure 2. ALES/ALAS configuration [2]

A typical abort event sequence is shown in Figure 1 and explained following:

1) Boost Phase: This is the initial stage where powerful rocket motors (main abort motors)(LM/HM) blast the crew capsule away from the launch vehicle in an emergency. Smaller steering motors help control the capsule's direction during this critical phase.

2) Coast Phase: After the initial thrust, the capsule enters a coasting phase where it glides freely. Here, only the steering motors (LACM/HACM) are used to maintain stability, keeping the capsule at a relatively shallow angle (low angle of attack) as it travels through the air.

3 & 4) Re-orientation Phases: These phases involve maneuvering the capsule into a safe position for re-entry. The steering motors turn the capsule from a position where it's stacked on top of the escape tower (tower-forward) to a position where the heat shield faces the

direction of travel (heat shield-forward). This is crucial for surviving re-entry into the atmosphere.

5) Tower Separation: Once the capsule is in the heat shield-forward position, the escape tower separates from the crew compartment (CM) using dedicated jettison motors. This allows the parachute system stored inside the crew compartment to deploy for a safe landing.

Before of integration and ground testing of ALEAS on the Crew Module of the launcher, the wind tunnel experiments using the active jet on the ALEAS model have an important impact for validation and development of system. To understand the aerodynamic forces acting on the launch vehicle and capsule during ascent, wind tunnel tests are performed using scaled models. These tests recreate the flight conditions by subjecting the models to simulated airflow under similitude conditions (Mach, Reynolds, and others). The resulting data aims to determine the forces (lift, drag, side force) and moments (pitch, roll, yaw) acting on the vehicle at different stages of the ascent. This information is crucial for designing and adjusting the launch vehicle's control systems to ensure its stability and proper attitude control throughout the critical ascent phase. This paper will focus on the development of the inner pneumatic system of model, including the design of nozzles and external feeding system. Additionally, representative instances of predicted wind tunnel outcomes (CFD) and FEA for structural validation of the entire assembly. Similar applications have been documented in numerous research facilities worldwide. These facilities employ jet rigs specifically designed to generate high-velocity airflows for jet engine simulations [2], [3], [7], [8], [9], [10].

2. SIMILITUDE PARAMETERS

For each jet line, the mass flow and total pressure have been calculated according to the similitude parameters described in [2] and showed below.

$$SP1 = \frac{\gamma_j M_e^2}{\gamma_\infty M_\infty^2} = \frac{\gamma_{jet_{real}} M_{jet_{real}}^2}{\gamma_{flight} M_{fligth}^2} \tag{1}$$

$$SP2 = \frac{\rho_e A_e V_e^2}{\rho_\infty A_e V_\infty^2} = \frac{\rho_{jet_{real}} A_{exit\ jet_{real}} V_{jet_{real}}^2}{\rho_{flight} A_{exit\ jet_{real}} V_{flight}^2} \tag{2}$$

$$SP3 = \frac{R_j T_e}{R_\infty T_\infty} = \frac{R_{jet_{real}} T_{s_{Jet_{real}}}}{R_{flight} T_{flight}} \tag{3}$$

where:

- $\gamma_j, \gamma_{jet_{real}}$ represents the heat specific ratio of the real jet gas
- $M_e, M_{jet_{real}}$ is the Mach number of the real jet
- $\gamma_\infty, \gamma_{flight}$ represents the heat specific ratio of the air
- $M_\infty,\ M_{flight}$ is the vehicle Mach number
- $\rho_e, \rho_{jet_{real}}$ is the jet gas density
- $\rho_\infty, \rho_{flight}$ is the air density
- $A_e, A_{exit\ jet_{real}}$ is the exit area of the real nozzle
- $V_{jet_{real}}$ represents the exit velocity of the real jets
- V_{flight} represents the velocity of vehicle
- $R_j, R_{jet_{real}}$ represents the gas constant of the real jet gas
- $T_e, T_{s_{Jet_{real}}}$ means the static temperature of the real jet gas exit

- T_{∞}, T_{flight} means the static pressure during the flight at a specific point

First similitude parameter (1) represents the plume boundary interaction of jets (exit pressure ratio), the second one (2) is the plume trajectory parameter (momentum flux ratio) and the third one (3) represents the plume entrainment (kinetic energy or velocity ratio).

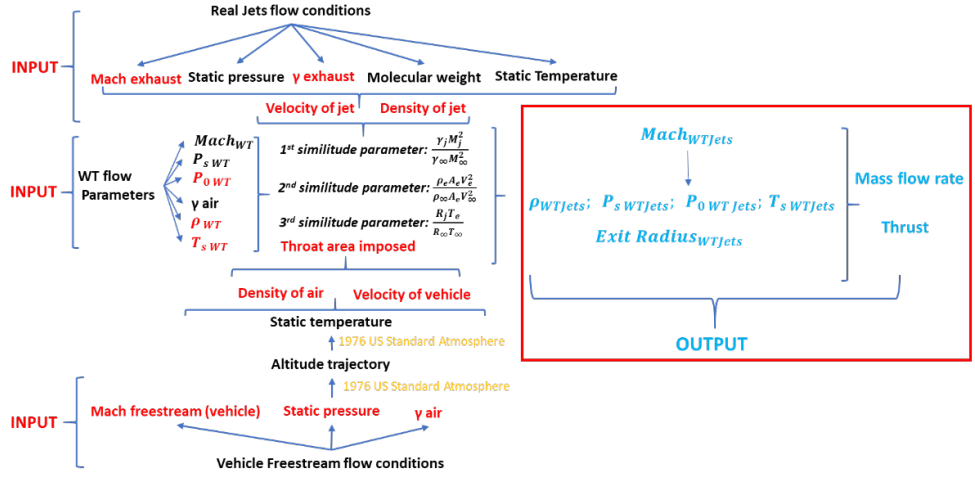

Figure 3. WT model nozzles parameters calculation algorithm

Figure 3 presents a computation algorithm for designing nozzles. This algorithm is detailed in the following equations:

$$M_{WTJet} = \sqrt{\frac{SP1 \cdot \gamma_\infty \cdot M_\infty^2}{\gamma_j}} \tag{4}$$

$$T_{S_{WTJet}} = \frac{T_{0_{WTJet}}}{1 + \frac{\gamma_j - 1}{2} M_{WTJet}^2} \tag{5}$$

$$V_{WTJet} = \sqrt{\gamma_{WTJet} \cdot R_{WTJet} \cdot T_{S_{WTJet}}} \tag{6}$$

$$\rho_{WTJet} = \frac{SP2 \cdot \rho_\infty \cdot V_\infty^2}{V_{WTJet}^2} \tag{7}$$

$$p_{S_{WTJet}} = \rho_{WTJet} \cdot R_{WTJet} \cdot T_{S_{WTJet}} \tag{8}$$

$$P_{0_{WTJet}} = p_{S_{WTJet}} \left(1 + \frac{\gamma_j - 1}{2} M_{WTJet}^2\right)^{\frac{\gamma_{WTJet}}{\gamma_{WTJet}-1}} [6] \tag{9}$$

$$A_{exit_{WTJet}} = A^* \cdot \frac{1}{2}(\gamma_{WTJet} + 1)^{-\frac{\gamma_{WTJet}+1}{2(\gamma_{WTJets}-1)}} \left(\frac{1 + \frac{1}{2}(\gamma_{WTJets} - 1) M_{WTJet}^2}{M_{WTJet}}\right)^{\frac{\gamma_{WTJet}+1}{2(\gamma_{WTJet}-1)}} [5] \tag{10}$$

$$\dot{m} = \frac{A_{total} \cdot p_{0_{WTJet}}}{\sqrt{T_{0_{WTJet}}}} \sqrt{\frac{\gamma_{WTJets}}{R}} \left(\frac{\gamma_{WTJets} + 1}{3}\right)^{-\frac{\gamma_{WTJets}+1}{2(\gamma_{WTJets}-1)}} [4] \tag{11}$$

$$Thrust = \dot{m} \cdot V_{WTJet} + \left(p_e - p_{0_{WTJet}}\right) \cdot A_{exit_{WTJet}}[4] \quad (12)$$

where,

- M_{WTJet} means the Mach number of the simulated jet during the wind tunnel test (WTT);
- The parameters with subscript *WTJet* are related to the wind tunnel jet conditions.

Achieving simultaneous testing conditions of all these scaling parameters using cold air proves to be impracticable. While it is feasible to align the momentum flux ratio and exit pressure ratio concurrently, achieving the desired velocity ratio presents a big challenge. Consequently, resorting to a gas simulant other than air or employing elevated temperatures becomes necessary. The utilization of cold air necessitates a trade-off: sacrificing higher mass flow at elevated velocities during flight for increased mass flow at slower speeds within the wind tunnel. The significance of the testing process varies based on the configuration, with the blockage effect predominating in many instances.

3. DESIGN OF THE ACTIVE RIG FOR THE WIND TUNNEL MODEL

To achieve realistic jet simulations during wind tunnel tests, a custom metal pneumatic line was developed and installed within the model. The design considerations for this component were as follows:

- *Compatibility with Force and Moment (F&M) Balance*: The pneumatic line needed to be positioned around the F&M balance, which is crucial for measuring aerodynamic loads exerted on the model during testing.
- *Maintaining Clearance*: There must be no physical contact between the model's outer shell and the internal pneumatic line to avoid interference and ensure accurate measurements.
- *Flow Parameter Accuracy*: The design ensures the jet airflow parameters precisely match the similitude parameters mentioned earlier, guaranteeing a realistic simulation of the actual jet flow.
- *Structural Integrity*: The pneumatic line prioritizes structural strength to comply with safety regulations and prevent damage to the model or expensive testing equipment.

The initial design aimed to be versatile, accommodating simulations for all jet types (LM, HM, LACM, HACM) simultaneously based on the abort scenario. However, a key drawback was its neglect of the second and third similitude parameters.

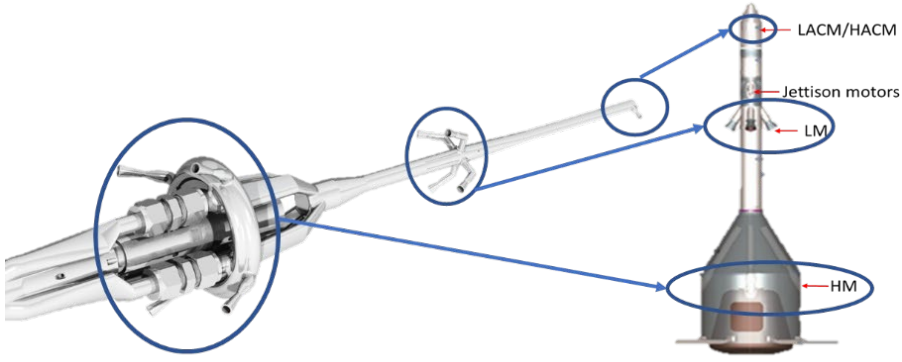

Figure 4. First iteration of the jet tree

To comply with the second similarity parameter, a redesign of the internal pneumatic system was implemented. This revised model design also offers the advantage of minimizing the likelihood of contact between the internal pneumatic components and the exterior of the model. However, the primary drawback encountered is related to achieving a sufficiently high mass flow rate, which presents a significant challenge. As a result, in this revised design, each jet type will operate independently due to the very high mass-flow rate. This isolation is essential to accommodate and maintain the integrity of the internal pneumatic system and to prevent any adverse effects on the aerodynamic measurements.

a) b)

Figure 5. Second design for the pneumatic tree: a) for Low Altitude Jets Config. and b) for High Altitude Jets config

4. COMPUTATIONAL FLUID DYNAMIC SIMULATIONS PERFORMED FOR EACH CONFIGURATION

To validate the flow characteristics both within the pneumatic network and at the outlets of each configuration, multiple numerical simulations were performed. The primary objectives of these analyses were as follows:

- *Validation of critical conditions at the imposed section*: This objective aimed to verify that the flow conditions at the designated section within the pneumatic network met the specified requirements, ensuring accurate flow representation.

- *Determination of pressure loss along the internal pneumatic circuit of the model*: This objective focused on quantifying the pressure drop experienced throughout the internal pneumatic network of the model. This information is crucial for evaluating the overall efficiency of the pneumatic system and identifying potential areas for improvement.

- *Verification of flow uniformity at the outlet of the nozzles*: This objective sought to confirm that the flow exiting the nozzles exhibited a uniform distribution across the outlet area. This uniformity is essential for ensuring consistent aerodynamic performance across the various configurations.

The numerical simulations employed a Reynolds-Averaged Navier-Stokes (RANS) model with the k-ε Realizable turbulence model to account for the turbulent effects in the flow. An implicit solver formulation was utilized for enhanced stability, particularly beneficial for steady-state simulations. The Roe-FDS scheme was selected for flux discretization due to its robustness and accuracy in capturing shock waves and complex flow phenomena. The least squares cell-based method was employed for the computation of variable flow gradients, ensuring a high degree of accuracy in the solution. Second-order upwind schemes were implemented for spatial discretization, providing a balance between accuracy and convergence characteristics. At the boundaries, pressure inlet and outlet conditions were imposed at the domain entrance and exit, respectively, to represent the inflow and outflow characteristics.

Adiabatic wall conditions were used for all walls, neglecting heat transfer between the fluid and the walls. The ANSYS Fluent 2022 software served as the computational platform for all the analyses. The governing equations in vector form used by RANS model are described below:

$$\frac{\partial}{\partial t}\iiint W dV + \oint [F - G] dA = \iiint H dV \tag{13}$$

where W is the conservative variables vector, F and G represents the convective and diffusive flux vectors and the vector H contains source terms such as body forces and energy sources:

$$W = \begin{Bmatrix} \rho \\ \rho u \\ \rho v \\ \rho w \\ \rho E \end{Bmatrix}, F = \begin{Bmatrix} \rho V \\ \rho V u + p\hat{\imath} \\ \rho V v + p\hat{\jmath} \\ \rho V w + p\hat{k} \\ \rho V E + pV \end{Bmatrix}, G = \begin{Bmatrix} 0 \\ \tau_{xi} \\ \tau_{yi} \\ \tau_{zi} \\ \tau_{ij} V_j + q \end{Bmatrix}, H = \begin{Bmatrix} 0 \\ \rho f_{ex} \\ \rho f_{ey} \\ \rho f_{ez} \\ \rho \overrightarrow{f_e} \overrightarrow{V} + \dot{q_h} \end{Bmatrix} \tag{14}$$

where ρ, u, v, w, V, E and $p$are the density, velocity components on each spatial direction, total velocity, total energy per unit mass and pressure of the fluid, moreover τ is the viscous stress tensor and q is the heat flux. The results showed that the main objectives were acceptable achieved. All details of the results are presented in the following pictures:

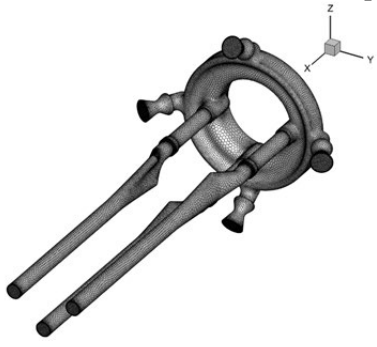

Figure 6. HM motors case :Surface grid

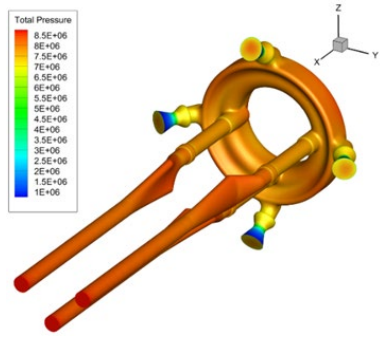

Figure 7. HM motors case: Pressure distribution on the walls

Figure 8. LM motors case: Surface computational domain

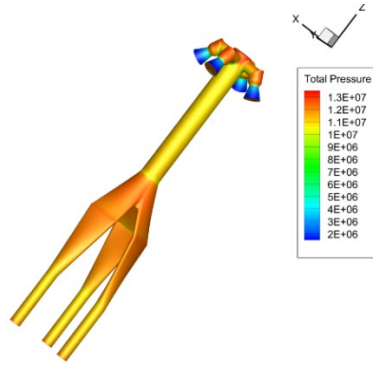

Figure 9. LM motors case: Pressure distribution on the walls

Analysis of the pressure distribution at the nozzle exits reveals a total pressure loss of approximately 10% for High Momentum (HM) motors and 21% for Low Momentum (LM) motors.

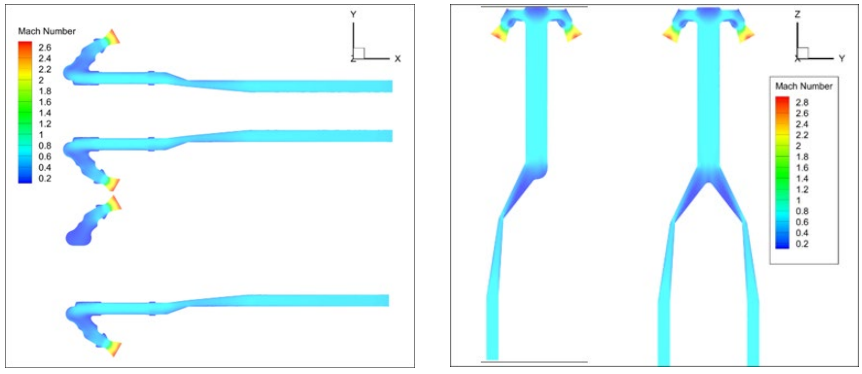

Figure 10. Mach number distribution on the symmetrical planes - Left is HM motors and Right is LM motors

Figure 10 illustrates that choked flow is present in the designated section for both configurations. Additionally, the figure provides a qualitative visualization of the Mach number distribution at the exit plane for each nozzle in both cases.

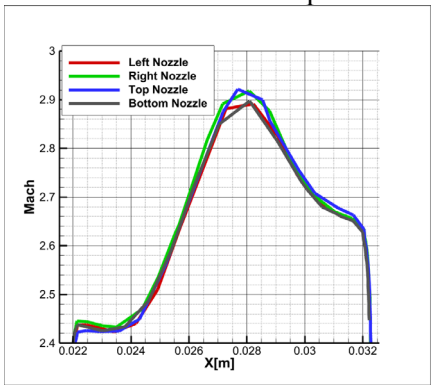

Figure 11. Mach distribution on outlet LM case

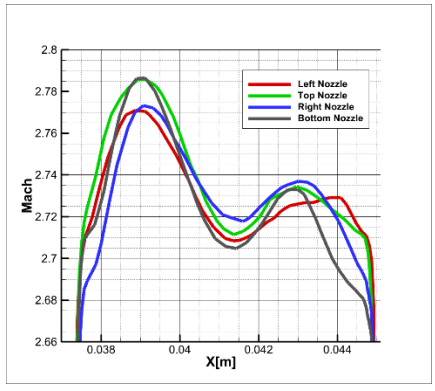

Figure 12. Mach distribution on outlet HM case

As illustrated in Figure 11 and Figure 12, the relative variation in Mach number at the exit exhibits a value of 3% for the HM case and 15% for the LM case. Furthermore, the achieved average Mach values deviate slightly from the target values, with a discrepancy of 1.4% for the HM case and 1.85% for the LM case.

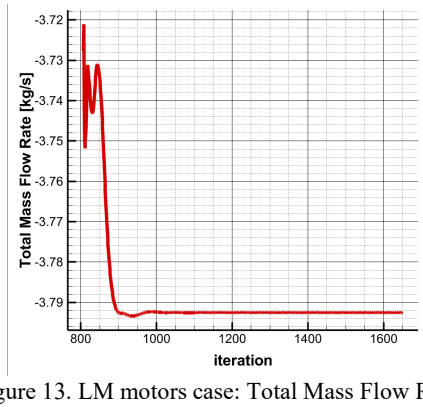

Figure 13. LM motors case: Total Mass Flow Rate convergence

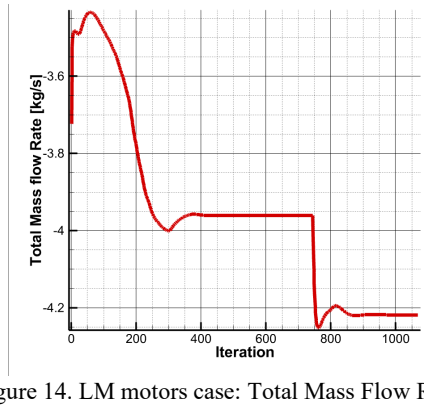

Figure 14. LM motors case: Total Mass Flow Rate convergence

Analysis of the total mass flow rate monitored at the domain exits for both HM and LM cases revealed a penalty of approximately 15% for the HM case and 12.5% for the LM case.

5. STRUCTURAL ANALYSES FOR VALIDATION OF DESIGN

To validate the structural integrity of the designed jet configurations, static linear finite element analyses (FEA) were conducted. These analyses employed a static linear solver, assuming a proportional relationship between stress and strain within the elastic regime. Contacts between components were modeled as linear, neglecting potential non-linear effects such as friction or adhesion. Pins and fasteners used in the assembly process were represented using RB2 type elements, which are well-suited for simulating the behavior of rigid connectors. ANSYS Static Structural 2022 software has been used as the computational platform for these simulations. Inconel 718 was chosen as the material for the pneumatic components due to its well-suited mechanical properties for Additive Layer Manufacturing (ALM), the fabrication technology employed for these parts. This selection is supported by Inconel 718's favorable characteristics, including a tensile strength (Rm) of 1300 MPa, yield strength (Rp0.2) of 1100 MPa, Young's modulus of 200 GPa, and Poisson's ratio of 0.3. Additionally, a material density of 7800 kg/m^3 was assigned. The loading conditions for both configurations were established based on the maximum total pressure of the jets realized during the test matrix.

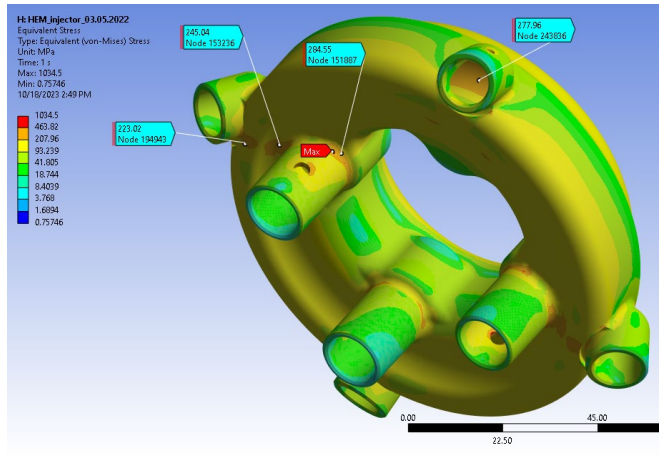

Figure 15. HM motors von-Misses stress distribution

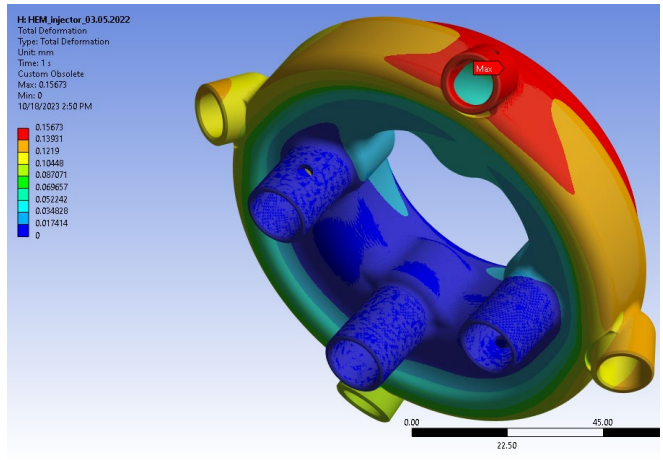

Figure 16. HM motors - Total Deformation

The finite element analysis (FEA) conducted for the HM case focused solely on the primary component of the assembly. This decision was justified by the successful validation achieved through the LM case analysis, which demonstrated the structural integrity of the remaining components within the pneumatic circuit. The analysis identified the core jet tree, which houses the jet nozzles, as the most critically loaded component for both the LM and HM configurations.

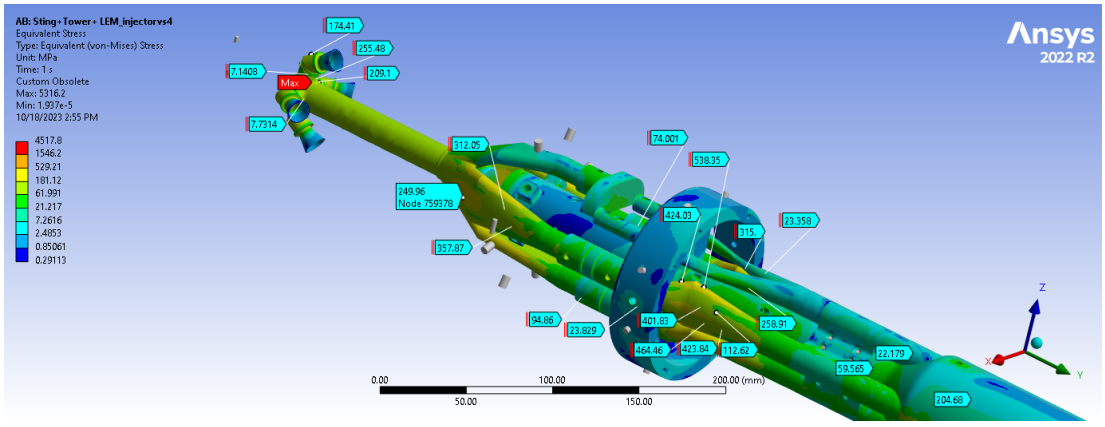

Figure 17. LM version von-Misses Stress Distribution

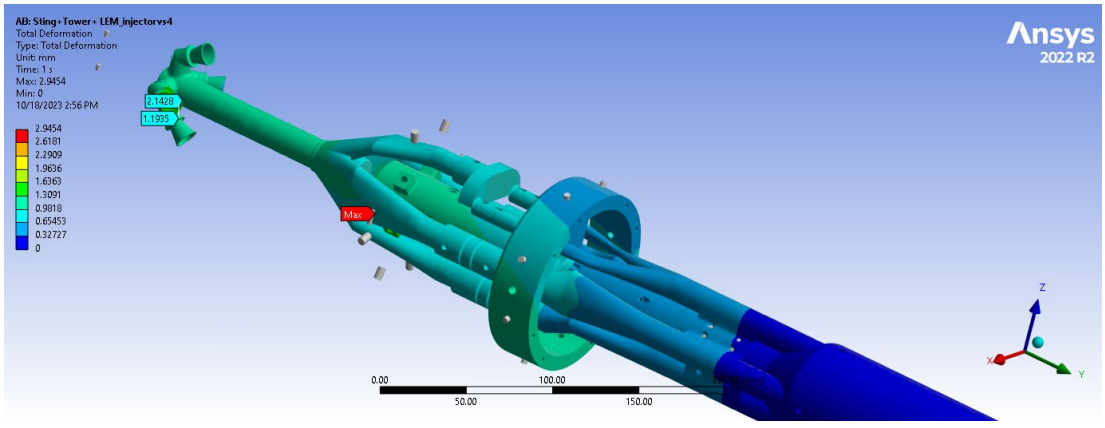

Figure 18. LM motors - Total Deformation

The results presented in Figure 15 - Figure 18 demonstrate that the entire assembly design satisfies the minimum safety factor (SF) requirement of 2.5. This finding indicates that the structure has a sufficient margin of safety to withstand the anticipated loads. Additionally, the observed total deformation validates the design constraint of preventing contact between the pneumatic tree and the model shell, ensuring proper functionality.

6. DESIGN OF THE HIGH PRESSURE JETS RIG DEDICATED FOR AN ACTIVE WIND TUNNEL MODEL

To ensure the pneumatic network's air supply during the aerodynamic experimental campaign, a dedicated air supply system was designed and partially fabricated to provide high-pressure and high mass-flow rate air to the nozzles of the test model. This system was structured into two main components: a chassis containing buffer tanks, pressure and temperature transducers,

solenoid valves for each supply line, high-pressure regulators, and a dedicated chassis for incorporating the buffer tank chassis and large-capacity tanks that ensured the necessary quantity for the experiments at the required flow rates.

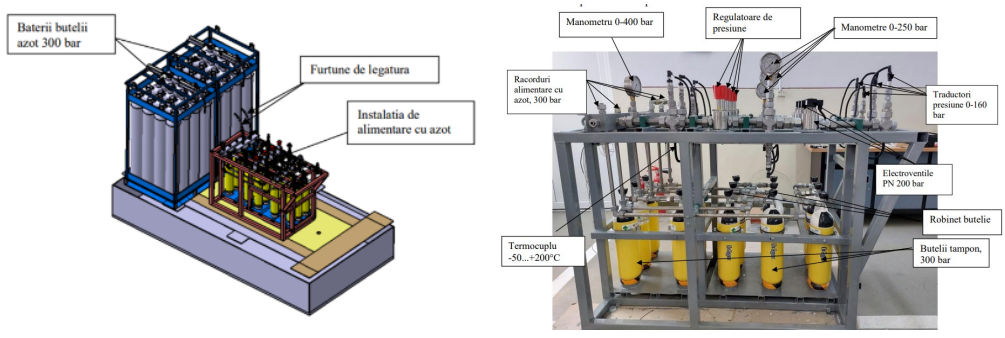

Figure 19. High pressure Jet rig developed by INCAS

Currently, only the buffer tank chassis has been fabricated, and its instrumentation is limited as shown in Figure 19.

The next stage of this research activity involves completing the instrumentation of the buffer tank and fabricating the large-capacity tank chassis. Subsequently, the large-capacity tank chassis will be integrated into the wind tunnel facility.

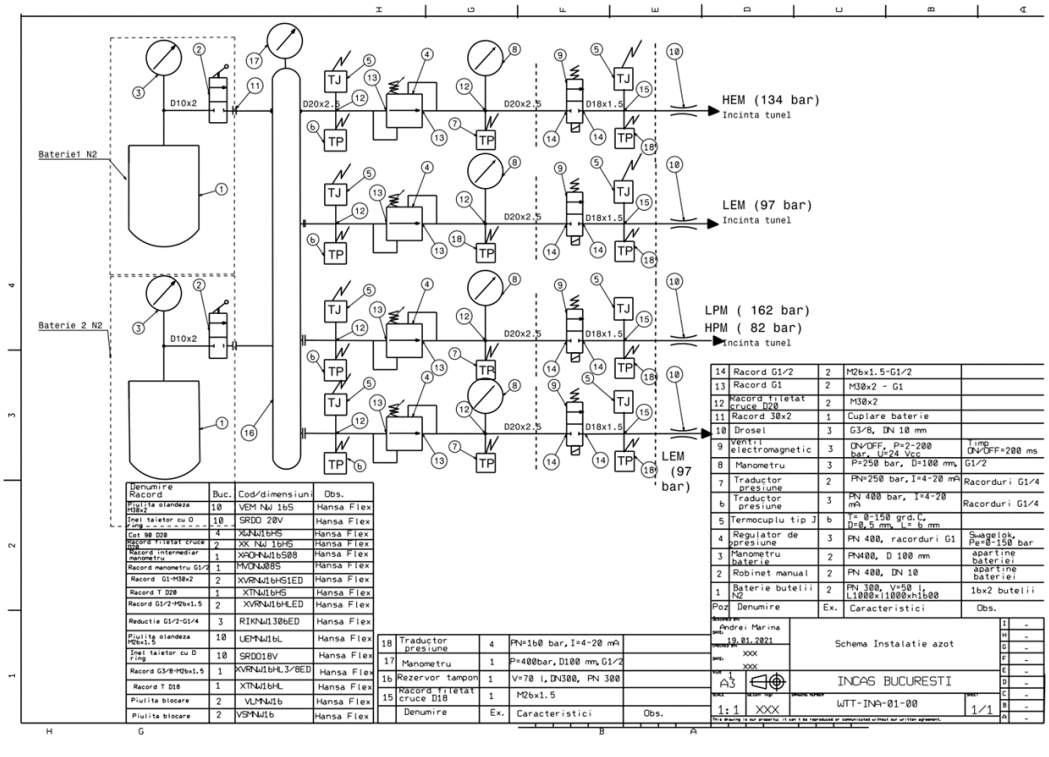

Figure 20. Technical Scheme of functionality of jet rig

The above figure reveals that the current instrumentation of the jet rig incorporates multiple levels, some of which may be redundant for efficient operation. However, the selected pressure regulator boasts a maximum capacity of 250 bar, enabling the compensation of pressure losses incurred throughout the complex pneumatic circuit.

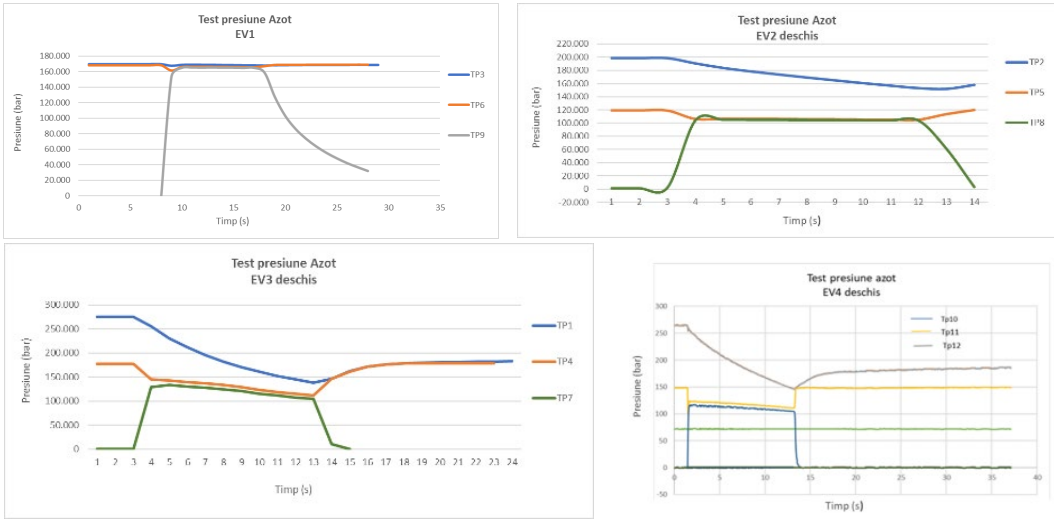

Figure 21. Initial discharge test of jet rig buffer tanks

The initial air discharge test demonstrated that all pressure regulators and transducers functioned according to the manufacturer's specifications.

7. CONCLUSIONS

The present research activity focuses on the development and validation of a novel wind tunnel test methodology for an active escape/abort system for aerospace vehicles. This methodology will be implemented within the INCAS wind tunnel facility and encompasses the following key stages:

Design of the Internal Pneumatic Assembly: A crucial aspect involves the design of the internal pneumatic assembly responsible for supplying the high-pressure and high-flow air required by the active escape/abort system. This assembly will likely integrate components such as buffer tanks, pressure regulators, and solenoid valves to ensure precise flow control and pressure regulation.

Development of the Dedicated Active Jets Rig: A dedicated active jets rig will be designed and fabricated to interface with the internal pneumatic assembly and the escape/abort system model. This rig will house the nozzles responsible for generating the thrust necessary for the escape/abort maneuver. The design will consider factors like nozzle geometry, flow uniformity, and structural integrity to ensure accurate simulation of the escape/abort sequence.

Validation of Functionality in Wind Tunnel Conditions: The final stage involves the validation of the escape/abort system's functionality under simulated wind tunnel conditions within the INCAS facility. This validation process will involve instrumentation of the system and the wind tunnel environment to acquire critical data on parameters such as forces, moments, and pressure distributions. The collected data will be used to assess the effectiveness of the escape/abort system and validate the accuracy of the wind tunnel test methodology.

This research effort aims to contribute to the advancement of wind tunnel testing methodologies for active escape/abort systems in the aerospace industry. The successful development and validation of this methodology will provide valuable insights into the performance of such systems under realistic wind tunnel conditions.

The present investigations have identified several critical challenges:

Confined Internal Space: The limited internal volume of the model imposes significant geometric constraints on the design, potentially impacting the accuracy of the simulation or test results.

Non-Contact Requirement for Force and Moment Measurements: The requirement for non-contact force and moment (F&M) measurements necessitates careful consideration of measurement techniques and potential limitations in capturing the complete interaction between the jets and the model.

Impractical Plume Entrainment Matching: Achieving perfect similitude based on the third dimensionless parameter may not be feasible within the limitations of the available wind tunnel facility heating system of the air used for jet simulation.

Operational Constraints on Jet Configuration: Operating all three jet configurations simultaneously while adhering to the first two similitude parameters might be impractical. This may necessitate alternative testing strategies or compromises in the test setup.

High Mass Flow Rate and Limited Measurement Window: The need to maintain similitude based on the second dimensionless parameter (often Mach number) can lead to significantly increased mass flow rates. This, in turn, can drastically reduce the experimental time window available for accurate F&M measurements.

REFERENCES

[1] J. Sreenivasulu, K. Saha, M. M. Patil & V. Ashok, Evolution of Crew Escape System configuration In *Current Science*, Vol. **120**, Issue 1, 2021.

[2] G. J. Brauckmann, J. S. Greathouse & M. E. White, (n.d.), Rocket Plume Scaling for Orion Wind Tunnel Testing, https://ntrs.nasa.gov/search.jsp?R=20110013236

[3] S. L. N. Desikan, R. Saravanan, K. Suresh, J. A. Tennyson, N. Chandrasekar, S. Subramanian & M. M. Patil, Effect of cold jet plume on aerodynamics coefficients, *Journal of Spacecraft and Rockets*, **52**(2), 404–415, 2015, https://doi.org/10.2514/1.A33086

[4] * * * Rocket Thrust Summary - NASA website. (n.d.), Https://Www.Grc.Nasa.Gov/Www/k-12/Airplane/Rktthsum.Html .

[5] * * * Mass Flow Choking - NASA Web Site. (n.d.), Https://Www.Grc.Nasa.Gov/Www/k-12/Airplane/Mflchk.Html .

[6] * * * Isentropic Flow - NASA Web Site, (n.d.), https://www.grc.nasa.gov/www/k-12/airplane/isentrop.html .

[7] H. H. Korst, R. A. White, S. E. Nyberg & J. Agrell, Simulation and modeling of jet plumes in wind tunnel facilities, *Journal of Spacecraft and Rockets*, **18**(5), 427–434, 1981, https://doi.org/10.2514/3.57837

[8] J. S. Draper, J. P. Moran, A Study of Wind Tunnel Simulation of High Altitude Rocket Plumes, Final Report, February 1973.

[9] J. Panda, G. H. James, N. J. Burnside, R. K. Fong, V. A. Fogt & J. C. Ross (n.d.), Use of Heated Helium to Simulate Surface Pressure Fluctuations on the Launch Abort Vehicle During Abort Motor Firing, Publication Date, June 5, 2011.

[10] K. Asai, NASA Reference Hot-Jet Simulation in Cryogenic Wind Tunnels, 1989, https://ntrs.nasa.gov/search.jsp?R=19890014077